Synthesis of Mixed Anion Rare Earth Sulfate Fluorides $Ln SO_4F \cdot H_2O$ (Ln = Nd, Tb, Dy, Ho) and $Ln SO_4F$ (Ln = Tb, Dy, Ho)

Lakshani W. Masachchi, Gregory Morrison, and Hans-Conrad zur Loye*

Department of Chemistry and Biochemistry, University of South Carolina, Columbia, SC, 29208, United States

*Corresponding author. E-mail: zurloye@mailbox.sc.edu

Abstract:

Single crystals of the mixed anion rare earth sulfate fluorides LnSO$_4$F•H$_2$O (Ln = Nd, Tb, Dy, and Ho), monoclinic space group $P2_1/n$, were prepared via an HF-free mild hydrothermal synthesis. Furthermore, the LnSO$_4$F (Ln = Tb, Dy, and Ho) phases, orthorhombic space group *Pnma*, were obtained via the thermal decomposition of LnSO$_4$F•H$_2$O (Ln = Tb, Dy, and Ho). While the LnSO$_4$F•H$_2$O (Ln = Nd, Tb, Dy, and Ho) phases are isostructural, two different structures are observed for the LnSO$_4$F (Ln = Tb, Dy, and Ho) series, one for Tb and one for Dy and Ho, differing in the rare earth coordination environments. Green photoluminescence is observed for Tb(SO$_4$)F•H$_2$O and Tb(SO$_4$)F. Magnetic measurements indicate the absence of magnetic order down to 2 K in the Ln(SO$_4$)F•H$_2$O and Ln(SO$_4$)F phases.

Introduction

Oxyfluorides often function as the foundation for many optical and magnetic materials[1,2], where one can observe that fluorides are distinct from other halides due to the difference in electronegativity, environmental stability, and their structural similarity to many oxide phases. In fact, fluoride and especially oxyfluoride structures are often similar to oxide structures due to oxygen and fluorine's similar sizes and electronegativities, which makes it relatively easy to combine these two elements within a single crystal structure. However, they differ due to their standard oxidation states, F = 1- vs O = 2-. The oxidation state difference has important implications for the elemental compositions that can be accommodated in otherwise structurally identical oxide vs fluoride materials and, in fact, can be used to tune oxidation states by adjusting the fluoride to oxide ratio in oxyfluoride materials.[3,4]

Many oxyfluorides are known in the literature, belonging to a wide variety of structure types that range from solid-state oxyfluorides, such as $Rb_4Ge_5O_9F_6$[5] and $BaWO_2F_4$[6], to salt inclusion phase fluorides, such as $[Ba_3F]Ta_4O_{12}F$,[7] to silicate oxyfluorides,[8,9] germanium oxyfluorides $Na_5Ln_4F[GeO_4]_4$ (*Ln* = Pr, and Nd),[10] phosphate fluorides, vanadyl fluorides, including $Sr_4V_3O_5F_{13}$, $Pb_7V_4O_8F_{18}$, $Pb_2VO_2F_5$, and Pb_2VOF_6,[11] and rare earth containing oxyfluorides, such as $Gd_4O_3F_7$,[12] $Lu_2O_3F_5$,[13] $Y_7O_6F_9$.[14] Such structures are of interest as optical hosts and for obtaining new magnetic materials. Oxyfluorides based on polyanions $ABXO_4F$, such as XO_4 = PO_4, ($Na_2M[PO_4]F$),[15] Mn_2PO_4F,[16] XO_4 = SiO_4, Mg_3SiO_4F,[17] $Cs_3RESi_4O_{10}F_2$,[18] XO_4 = GeO_4, $NaCa_2GeO_4F$,[19] $V_2GeO_4F_2$,[20] and XO_4 = VO_4, Mn_2VO_4F[21] are known and recently XO_4 = SO_4 based phases have been reported, such as $Ce(SO_4)F_2•H_2O$,[22] $Na_4TiF_4(SO_4)_2$,[23] $KYb(SO_4)F_2$,[24] $LiLa_2F_4(SO_4)_2$,[25] and $GdSO_4F$.[26]

Many sulfate fluorides have been synthesized using the mild hydrothermal synthesis method, typically involving HF as a fluorinating agent,[27–30] while a few other systems, such as carbonate fluorides, also could be obtained under HF-free conditions.[31] Recently, Wu *et.al* reported the HF-free synthesis of $Ce(SO_4)F_2•H_2O$ using ZnF_2 as a fluorinating agent.[22] Using a similar HF-free approach, in our efforts to extend this approach from Ce to the other lanthanides, we, however, obtained different products, namely the *Ln*(III) containing $Ln(SO_4)F•H_2O$ reported herein, vs the Ce(IV) containing $Ce(SO_4)F_2•H_2O$ reported by Wu.[22] We extended our results to $Ln(SO_4)F•H_2O$ (*Ln* = Nd, Tb, Dy, and Ho) and, via a thermal decomposition route, were able to also obtain $LnSO_4F$ (*Ln* = Tb, Dy, and Ho). The structures and properties of these new phases are discussed herein.

Experimental

Synthesis

Materials: Nd_2O_3 (99.9%, Acros Organics), Dy_2O_3 (99.9%, Alfa Aesar), Ho_2O_3 (99.9%, Alfa Aesar), $Tb_2(SO_4)_3$•$8H_2O$ (99.9%, Thermo Scientific), H_2SO_4 (36N, Fisher) and ZnF_2 (99.9%, Alfa Aesar) were used as received.

Ln$(SO_4)F$•H_2O (*Ln* = Nd, Tb, Dy, and Ho) were prepared hydrothermally. A mixture of Ln_2O_3 (*Ln* = Nd, Dy, and Ho) or $Tb_2(SO_4)_3$•$8H_2O$ (0.8 mmol), ZnF_2 (1.8 mmol), H_2SO_4 (0.4 mL), and deionized water (1 mL) were sealed into a PTFE lined autoclave (23 mL). The autoclave was heated to 230 °C at 10 °C/min in a programmable convection oven, allowed to dwell for 72 hours, and cooled to room temperature at a rate of 3 °C/h. The polycrystalline powders were isolated *via* vacuum filtration and washed with water and acetone.

Polycrystalline powders of *Ln*$(SO_4)F$ (*Ln* = Tb, Dy, and Ho) were prepared by the thermal decomposition of *Ln*$(SO_4)F$•H_2O samples at 500 °C inside a tube furnace under N_2 flow.

Single-Crystal X-ray Diffraction (SXRD)

X-ray intensity data were collected on *Ln*$(SO_4)F$•H_2O (*Ln* = Nd, Tb, Dy, and Ho) at 298(2) or 301(2) K using a Bruker D8 QUEST diffractometer equipped with a PHOTON-II area detector and an Incoatec microfocus source (Mo Kα radiation, λ = 0.71073 Å). The crystals were mounted on a microloop using immersion oil. The raw area detector data frames were reduced and corrected for absorption effects using the SAINT+ and SADABS programs.[32,33] Final unit cell parameters were determined by least-squares refinement. Initial structural models were obtained with SHELXT. Subsequent difference Fourier calculations and full-matrix least-squares refinement against F^2 were performed with SHELXL-2018 using Olex2.[34] The crystallographic data and results of the diffraction experiments are summarized in Table 1.

Powder X-ray Diffraction (PXRD)

Powder X-ray diffraction data were collected on a Bruker D2 Phaser powder X-ray diffractometer using Cu Kα radiation to confirm the phase purity of polycrystalline samples obtained by grinding single crystals (Figure S1 and S2). The data were collected in the angular range 5–65° 2θ in steps of 0.04° over 120 minutes. The presence of preferred orientation (0 0 2)

was revealed in the PXRD analysis of the *Ln*(SO_4)F (*Ln* = Tb, Dy, and Ho) patterns; this information was used in the Rietveld refinement.

PXRD data for the Rietveld refinement of *Ln*(SO_4)F (*Ln* = Tb, Dy, and Ho) were collected on a Rigaku Ultima IV diffractometer equipped with a Cu Kα X-ray source and a DteX Ultra detector over a 2θ range of 5−120° with a step size of 0.02° and a scan rate of 0.2°/min. The diffraction patterns were analyzed, fitted, and refined with the Rietveld/d-I pattern method using the TOPAS v5 software for structure determination.

Rietveld Refinement

Rietveld refinements on *Ln*(SO_4)F (*Ln* = Tb, Dy, and Ho) were performed operating TOPAS commercial v5 in launch mode using jEdit with macros for TOPAS.[35] The default approach was refining the unit cell parameters, the Gaussian and Lorentzian isotropic size parameters, scale factors, and Chebychev background parameters. The occupancies, temperature factors, and atomic positions were fixed according to the isostructural Gd(SO_4)F CIF obtained from SXRD.[26] A high-order spherical harmonic intensity correction was needed to refine the peak shapes. Crystallographic information for the Rietveld refined structures is provided in Table 2.

IR spectroscopy

Vibrational spectra over the range of 4000–650 cm^{-1} were recorded using a PerkinElmer spectrum 100 FT-IR spectrometer equipped with a diamond ATR attachment (Figure S3).

Thermogravimetric Analysis

Thermogravimetric and differential thermal analysis (TGA/DTA) measurements were performed on polycrystalline powder samples using a TA Instruments SDT Q600 Thermogravimetric Analyzer and a platinum pan as the sample holder. Samples were heated from room temperature to the target temperature (500 °C) at 10 °C/min under a flow of nitrogen gas (100 mL/min), and the resulting powders were analyzed by PXRD for phase identification post-heating.

PL Measurements

PL emission spectra were collected on single crystals of Tb(SO_4)F•H_2O using a HORIBA Scientific Standard Microscope Spectroscopy System connected with iHR320 spectrometer and

synchrony detector operating on LabSpec 6 software. Spectra were recorded from 400 to 750 nm using 375 nm laser excitation source power 0.5 mW with 10× UV objective.

Magnetic Measurements

Susceptibility and magnetization measurements were performed on ground single crystals using a Quantum Design MPMS3 SQUID magnetometer. Susceptibility measurements were collected under zero-field cooled (ZFC) and field-cooled (FC) conditions in the temperature range of 2−300 K at an applied field of 0.1 T. The raw data were corrected for radial offset and shape effects.[36]

Table 1. Crystallographic data for $Ln(SO_4)F•H_2O$ (*Ln* = Nd, Tb, Dy, and Ho).

	$Nd(SO_4)F•H_2O$	**$Tb(SO_4)F•H_2O$**	**$Dy(SO_4)F•H_2O$**	**$Ho(SO_4)F•H_2O$**
Formula weight	277.32	293.00	295.58	298.01
Temperature, K	298(2)	299(2)	299(2)	298(2)
Crystal system	monoclinic			
Space group, Z	$P2_1/n$			
a, Å	5.0307(1)	4.9916(1)	4.9849(1)	4.9747(1)
b, Å	7.4919(1)	7.3513(1)	7.3322(1)	7.3113(1)
c, Å	11.8940(2)	11.6210(2)	11.5662(2)	11.5158(2)
β, deg	96.129(1)	96.714(1)	96.82788(1)	96.855(1)
Volume, $Å^3$	445.717(13)	423.505(13)	419.750(13)	415.853(12)
ρ_{calc}, g/cm^3	4.133	4.580	4.677	4.760
μ/mm^{-1}	12.068	17.140	18.246	19.475
F(000)	508.0	508.0	532.0	536.0
Crystal size, mm^3	0.07 × 0.06 × 0.01	0.05 × 0.03 × 0.01	0.03 × 0.06 × 0.01	0.05 × 0.03 × 0.01
Radiation (λ, Å)	0.71073			
2θ range, deg.	6.438 – 72.674	6.572 – 72.676	6.592 – 72.680	6.614 – 72.726
Reflections collected	55652	47452	57323	46700
Data/restraints/parameters	2158/0/82	2058/0/75	2044/0/75	2021/0/75
Goodness-of-fit	1.145	1.150	1.260	1.143
R_1 [I>=2σ(I)]	0.0143	0.0091	0.0095	0.0100
wR_2 [all data]	0.0450	0.0225	0.0226	0.0230
Largest diff. peak/hole, e $Å^{-3}$	1.04/–0.73	0.57/–0.61	0.66/–0.69	0.58/–0.60
R_{int}, %	2.83	3.56	3.51	4.08

Table 2. Crystallographic data for Rietveld structure refinements of $Ln(SO_4)F$ (*Ln* = Tb, Dy, and Ho).

	$TbSO_4F$	**$DySO_4F$**	**$HoSO_4F$**
Crystal system	orthorhombic	orthorhombic	orthorhombic
Space group, Z	*Pnma*	*Pnma*	*Pnma*
a, Å	8.3800(1)	8.3384(1)	8.3123(1)
b, Å	6.9863(1)	6.9576(1)	6.9234(1)
c, Å	6.4178(1)	6.3973(1)	6.3768(1)
R_{wp} (%)	1.54	1.33	2.27
R_p (%)	1.04	0.90	1.45
GOF	2.51	3.32	3.75

Results and Discussion

Synthesis

We successfully synthesized a novel series of sulfate fluorides, $Ln(SO_4)F•H_2O$ (*Ln* = Nd, Tb, Dy, and Ho), using ZnF_2, instead of $HF_{(aq)}$, as the fluorinating agent. Using metal fluorides as fluorinating agents is much safer (compared to HF) and slows down the immediate fluorination of solution species. This can avoid, or minimize, the precipitation of unwanted byproducts, such as binary or ternary fluorides, which often result from the use of potent fluorinating agents like HF(aq).[31] Therefore, this synthesis approach further supports that metal fluorides hold great potential as fluorinating agents to obtain pure phases of sulfate fluorides.

Heating $Ln(SO_4)F•H_2O$ to 500 °C eliminates the water of hydration and results in the anhydrous $Ln(SO_4)F$ (*Ln* = Tb, Dy, and Ho) phases. The heating process was carried out inside a tube furnace under N_2 flow to prevent the fluoride samples from reacting with atmospheric oxygen.[37]

Crystal Structure Description

Crystal structures of $Ln(SO_4)F•H_2O$ (*Ln* = Nd, Tb, Dy, and Ho) were determined by SXRD. Block-shaped crystals of $Nd(SO_4)F•H_2O$ (Figure 1), $Tb(SO_4)F•H_2O$, $Dy(SO_4)F•H_2O$ and $Ho(SO_4)F•H_2O$ were isolated from the mild hydrothermal synthesis with a yield of 91%, 84%, 87%, and 81%, respectively, based on *Ln*.

All these compounds are isostructural and crystallize in the monoclinic space group $P2_1/n$. The three-dimensional framework of all compositions consists of an asymmetric unit of one *Ln* atom, one S atom, one F atom, five O atoms and two H atoms. *Ln* is coordinated to six oxygen and two fluorine atoms forming a $[LnO_6F_2]$ polyhedron (Figure 2a). These polyhedra are connected to each other by edge-sharing via one fluorine and one oxygen atom and form one-dimensional (1D) chains along the *b*-direction (Figure 2b). These chains are linked to each other by intervening SO_4 tetrahedra, resulting in a three-dimensional framework. Each SO_4 tetrahedra is connected via three oxygens to one chain and via the fourth vertex to the adjacent chain (Figure 2c). The remaining O vertex of the $[LnO_6F_2]$ polyhedron, which is not bound to S, belongs to the water molecule, which terminates that vertex (Figure 2d).

Figure 1. Picture showing representative crystals of $Nd(SO_4)F•H_2O$

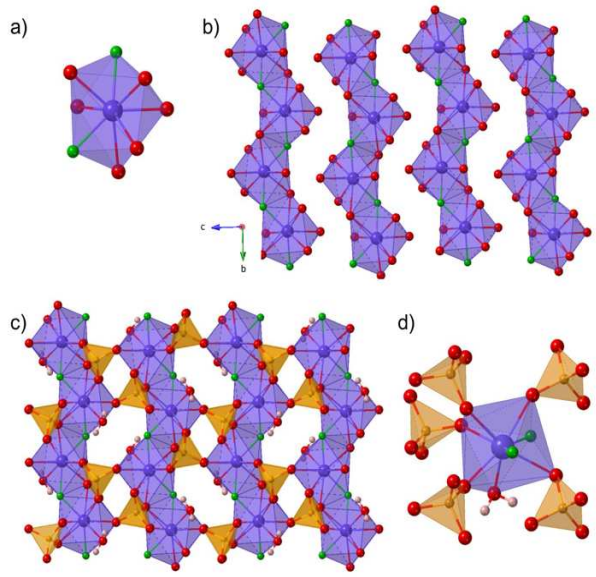

Figure 2. View of the monoclinic *Ln*$(SO_4)F•H_2O$ crystal structure

Thermal Properties

The thermal behavior of the compounds, **1−4**, was explored to study the structural stability of *Ln*$(SO_4)F•H_2O$ upon heating. The TGA curves reveal rapid weight loss over the temperature range of 350 °C to 450 °C, which corresponds to the loss of water (Figure 3). The total weight losses are 7.5, 6.6, 6.0, and 6.1 wt% for compounds $Nd(SO_4)F•H_2O$, $Tb(SO_4)F•H_2O$, $Dy(SO_4)F•H_2O$, and $Ho(SO_4)F•H_2O$, respectively, which are in good agreement with the calculated values of 6.54, 6.16, 6.08, and 6.04 wt% corresponding to the loss of one water molecule.

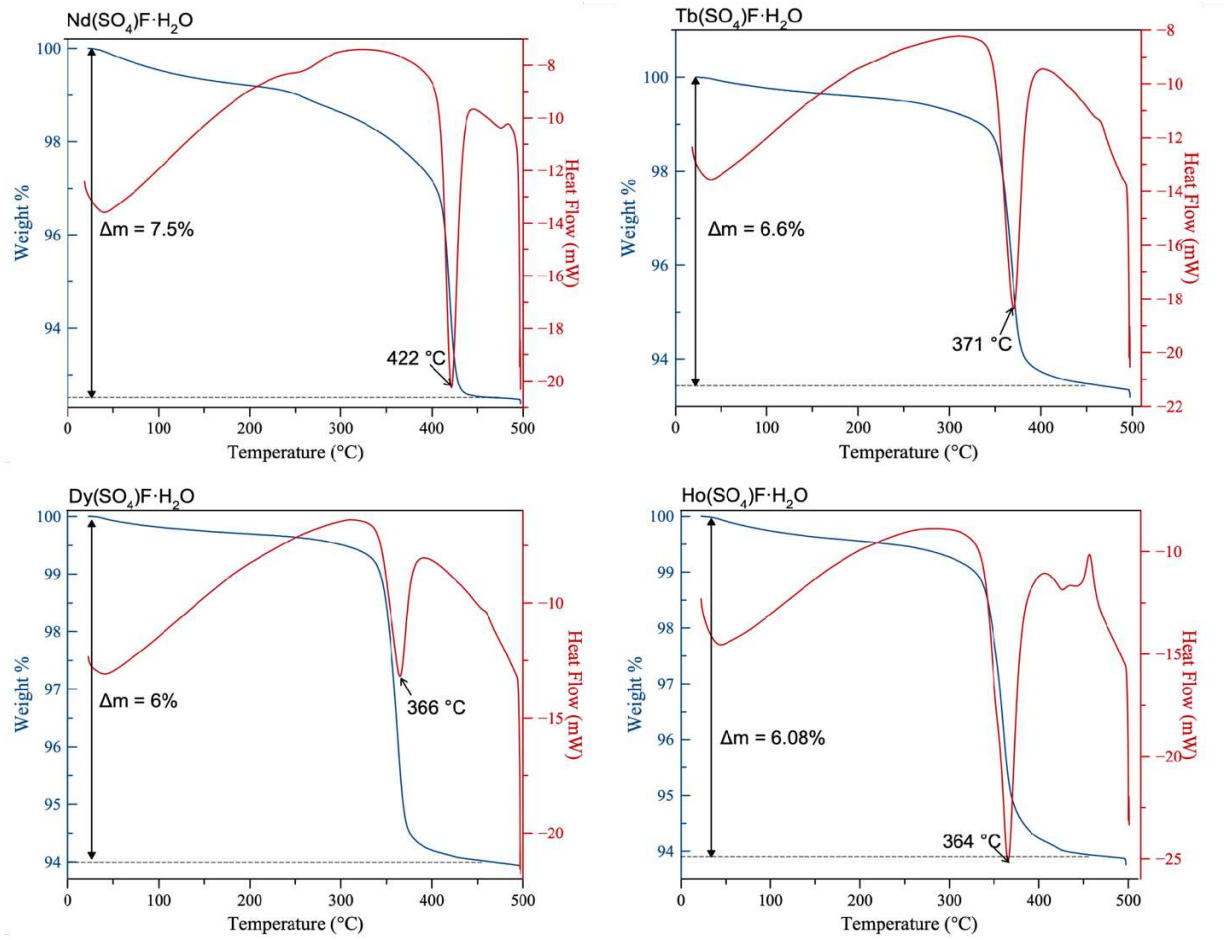

Figure 3. Thermogravimetric and differential thermal analysis plots.

The DTA data reveal a strong endothermic peak at 371 °C, 366 °C and 364 °C for $Tb(SO_4)F•H_2O$, $Dy(SO_4)F•H_2O$, and $Ho(SO_4)F•H_2O$, respectively. This thermal event corresponds to the structure transformation from monoclinic $Ln(SO_4)F•H_2O$ to orthorhombic $Ln(SO_4)F$ (Figure S2) and corresponds to the loss of water molecules at around 350−400 °C with a concomitant increase in the symmetry of the crystal structure. On the other hand, $Nd(SO_4)F•H_2O$ decomposed to $Nd_2(SO_4)_3$ and NdF_3 just above 400 °C, as indicated by the peak at 422 °C in the DTA plot. PXRD of the post-TGA products confirmed the structure transitions (Tb, Dy, Ho) and decomposition (Nd) of the phases. It is likely that the difference in the lanthanide ionic radii plays a role in the stability of the $Ln(SO_4)F$ (*Ln* = Tb, Dy, and Ho) versus the potential Nd composition that did not form due to complete decomposition rather than dehydration when heating $Nd(SO_4)F•H_2O$ above 400 °C.

Crystal structures of *Ln*(SO_4)F (*Ln* = Tb, Dy, and Ho) polycrystalline samples were confirmed via Rietveld refinement (Figure 4), where the structure of Gd(SO_4)F [26] was used as the structure model. Table 2 contains the values for the refined unit cells as well as Rp, Rwp, and GOF for the refinements. The low values of the reliability parameters (Rp, Rwp, and GOF) demonstrate the excellent fit of the data. Crystallographic information for the Rietveld refined structures is provided in Table S1.

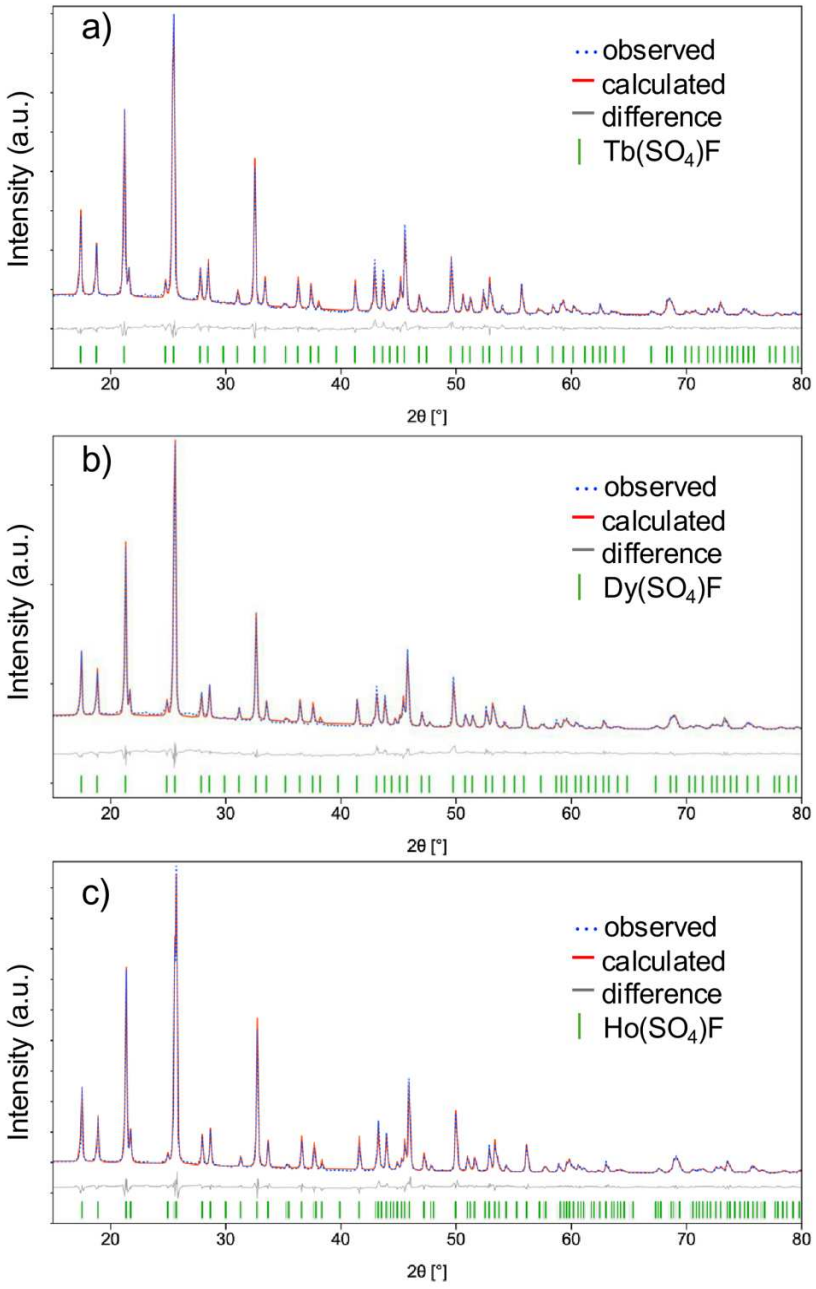

Figure 4. Rietveld refinement plots of $TbSO_4F$ (a), $DySO_4F$ (b), and $HoSO_4F$ (c); red line is the Rietveld fit, blue •'s are the observed PXRD data, grey line is the residual, and the vertical green tick marks indicate the allowed Bragg reflections.

Anhydrous *Ln*$(SO_4)F$ (*Ln* = Tb, Dy, and Ho) crystalize in the centrosymmetric space group *Pnma* in the orthorhombic crystal system. Although all compounds in the *Ln*$(SO_4)F$ series crystallize in the same space group, a slight difference in the coordination environment of the *Ln*

ions is known to exist. The rare earth coordination environment can be described either as being eightfold coordinated by six O atoms and two F atoms or as having a 6 + 2 coordination environment consisting of four O atoms and two F atoms and two longer Ln-O contacts. In the literature, $Y(SO_4)F$ is described with Y having a 6 + 2 coordination environment, and $Gd(SO_4)F$ is described with Gd having a coordination number of 8.[26,38] Based on the Ln–O bond lengths, we can describe the three structures either as having CN = 8 (Figure 5) or with a 6 + 2 coordination environment (Figure 6) as the ionic radii of Tb (0.923 Å), Dy (0.912 Å), and Ho (0.901 Å) fall right between the sizes of Gd (0.938 Å) and Y (0.900 Å). If we describe the $Tb(SO_4)F$ structure, containing the largest of the 3 rare earths, in the $Gd(SO_4)F$ structure, then each Tb atom is eightfold coordinated by six O atoms and two fluoride atoms.[26] These $[TbO_6F_2]$ units form chains by edge-sharing oxygen atoms. Unlike in $Ln(SO_4)F•H_2O$ where the chains are isolated and connected only via SO_4 units, the adjacent Tb polyhedral chains in this structure type are connected to each other via corner-shared fluorides. Each polyhedral chain is linked to four neighboring chains through fluoride vertices (Figure 5a) and is additionally interconnected by both corner-sharing and edge-sharing sulfate (SO_4) tetrahedra (Figure 5b), making $Tb(SO_4)F$ a more compact structure compared to $Tb(SO_4)F•H_2O$.

In contrast to $TbSO_4F$, if we describe $DySO_4F$ and $HoSO_4F$ in the 6 + 2 $Y(SO_4)F$ structure, then Dy and Ho exhibit octahedral connectivity with two fluorides and four oxides.[38] These very distorted LnO_4F_2 octahedra are connected via the trans fluoride vertices and form 1D LnO_4F_2 chains along the *a*-direction (Figure 6a). These chains are connected to each other only via corner-sharing SO_4 tetrahedra, where each SO_4 anion is connected to four LnO_4F_2 octahedra, to form a 3d network (Figure 6b).

We observed that the unit cell volume decreases linearly from the Nd to the Ho composition in $Ln(SO_4)F•H_2O$. The measured unit cell volume was plotted against the cubed ionic radii of the rare-earth atoms in an eight-coordinate environment obtained from the Shannon ionic radii database (Figure 7).[39] It is important to note that despite the lanthanide contraction, all materials represented by the formula $Ln(SO_4)F•H_2O$ exhibit the same crystal structure. However, for $Ln(SO_4)F$ compositions, Tb^{3+} exhibits eight coordination, whereas Dy^{3+} and Ho^{3+} are characterized by six coordination environments. This highlights the adaptability of certain crystal systems like $Ln(SO_4)F•H_2O$ to accommodate differently sized cations, while preserving a consistent coordination environment and structural connectivity,[31] in contrast with other compositions, such

as *Ln*(SO_4)F, which illustrate a change in the lanthanide coordination environment due to the change in the size of the lanthanide when moving across the series.[40]

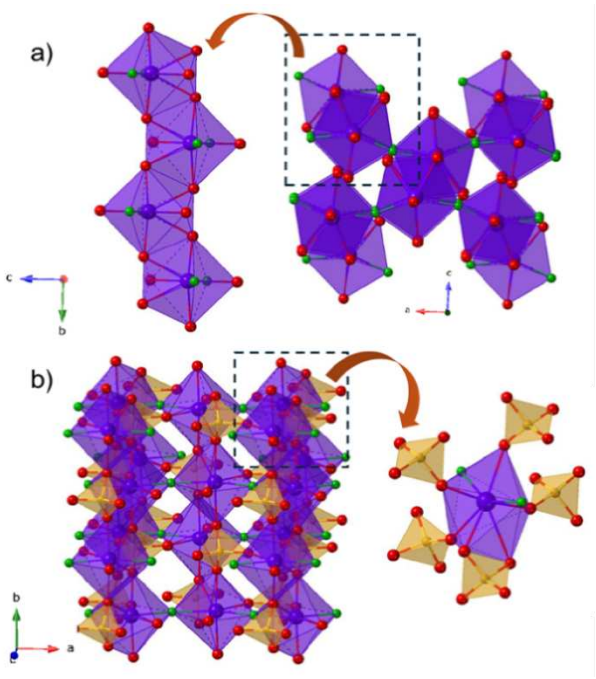

Figure 5. View of the orthorhombic Gd(SO_4)F crystal structure

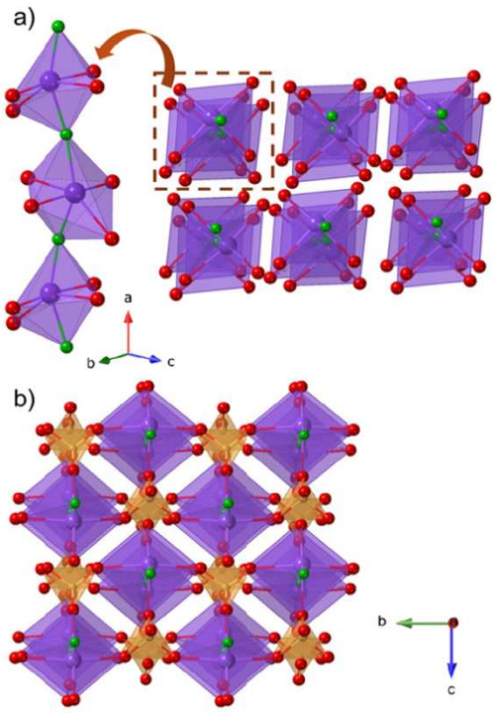

Figure 6. View of the orthorhombic $Y(SO_4)F$ crystal structure

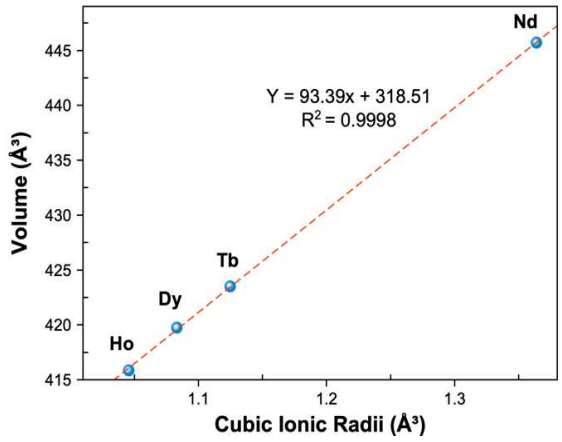

Figure 7. Unit cell volume vs rare-earth cubic ionic radii plot for $Ln(SO_4)F{\bullet}H_2O$ compounds

IR Spectroscopy

As shown in Figure S3, the IR spectra of $Ln(SO_4)F{\bullet}H_2O$ readily verifies the presence of the SO_4 moiety. The absorption peaks observed at 1200−1010 cm^{-1} are assigned to the asymmetric stretching vibration of $[SO_4]$. The broad absorption bands centered at 3470 cm^{-1} are due to the presence of H_2O molecules and absorption bands appearing at 1600 cm^{-1} are attributed to H-OH bending modes.[41]

Photoluminescence

Tb^{3+} is well known to exhibit green photoluminesce and, therefore, PL emission spectra were collected on $Tb(SO_4)F{\bullet}H_2O$ and $Tb(SO_4)F$ crystals. $Tb(SO_4)F{\bullet}H_2O$ and $Tb(SO_4)F$ exhibit characteristic 4f–4f electronic transitions, as illustrated in Figure 8. Both samples exhibit broad peaks at 490, 541, 584, and 618 nm, corresponding to $^5D_4 \rightarrow {}^7F_6$, $^5D_4 \rightarrow {}^7F_5$, $^5D_4 \rightarrow {}^7F_4$, and $^5D_4 \rightarrow {}^7F_3$ transitions, respectively. The $^5D_4 \rightarrow {}^7F_5$ transition, at 542 nm for $Tb(SO_4)F{\bullet}H_2O$ and 540 nm for $Tb(SO_4)F$, dominates the PL emission spectrum, resulting in a green-colored luminescence that agrees well with previously reported Tb-doped materials.[31,36,42]

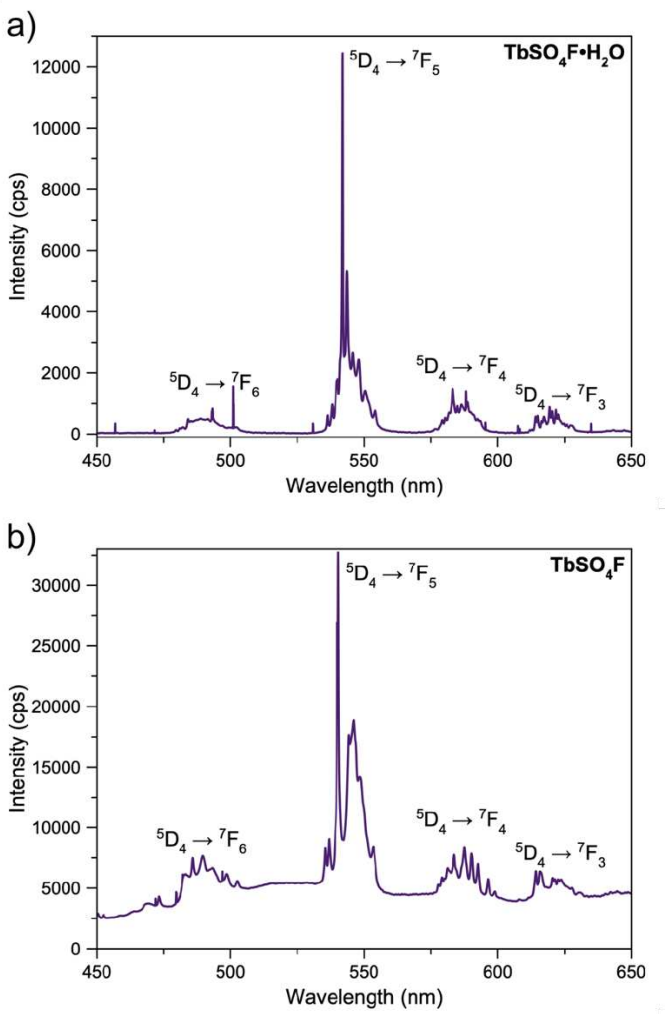

Figure 8. PL emission spectrum collected from a single crystals of $Tb(SO_4)F•H_2O$ and Tb(SO4)F

Magnetism

The crystal structures of *Ln*$(SO_4)F•H_2O$ and *Ln*$(SO_4)F$ contain chains of edge-sharing rare earth polyhedra. As Nd, Tb, Dy, and Ho possess 3, 6, 5, and 4 unpaired f electrons, respectively, we were interested in determining if this resulted in any f-f electron interactions and potential long-range magnetic orders. Although many rare-earth sulfate fluorides do not exhibit long-range magnetic order due to weak 4f–4f magnetic interactions, compounds like $KYb_2F_5(SO_4)$ have shown interesting magnetic properties in the literature.[43] Therefore, to explore this possibility, we performed magnetic susceptibility measurements on samples of $Ho(SO_4)F•H_2O$, $Ho(SO_4)F$, and $Tb(SO_4)F$ over the temperature range 2–300 K. These samples were selected in order to represent all the different structures associated with the *Ln*$(SO_4)F•H_2O$ and *Ln*$(SO_4)F$ series. The materials,

as shown in Figure 9, do not display long-range magnetic order and exhibit paramagnetic behavior down to 2 K. The magnetic susceptibility curves of these compounds follow Curie–Weiss behavior with small Weiss constants (Figure 9). The magnetic data for $Ho(SO_4)F•H_2O$, $Ho(SO_4)F$, and $Tb(SO_4)F$ are summarized in Table 3. The observed magnetic moments agree well with the calculated moments for all materials. According to the literature, many rare-earth sulfate fluorides do not exhibit long-range magnetic order due to weak 4f–4f magnetic interactions.[41]

Table 3. Magnetic Properties of $Ho(SO_4)F•H_2O$, $Ho(SO_4)F$, and $Tb(SO_4)F$.

Chemical Formula	Magnetic Properties	Effective magnetic moment (μ_{eff}) (μ_B/F.U.)		θ_{CW} (K)
		observed	calculated	
$Ho(SO_4)F•H_2O$	paramagnetic	10.68	10.60	–8.70
$Ho(SO_4)F$	paramagnetic	10.49	10.60	–2.24
$Tb(SO_4)F$	paramagnetic	9.75	9.70	–4.21

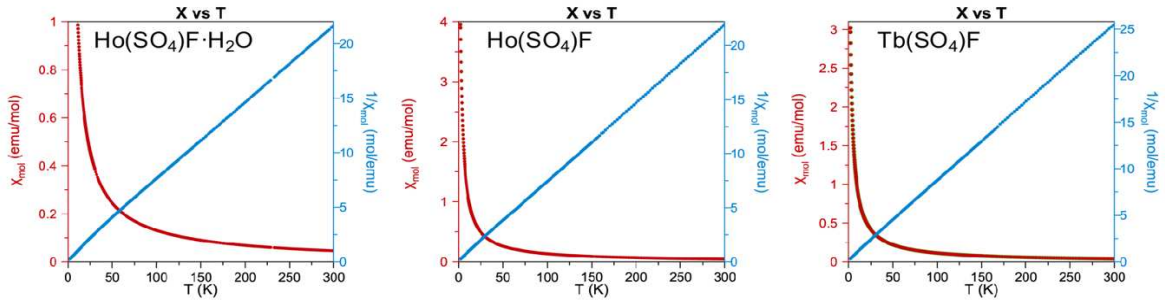

Figure 9. DC molar magnetic susceptibility (χ_{mol}) and inverse susceptibility ($1/\chi_{mol}$) vs. temperature plots for $Ho(SO_4)F•H_2O$, $Ho(SO_4)F$, and $Tb(SO_4)F$.

Conclusion

Single crystals of the mixed anion rare earth sulfate fluorides *Ln*(SO4)F•H2O (*Ln* = Nd, Tb, Dy, and Ho) were prepared via an HF-free mild hydrothermal synthesis, while the *Ln*SO4F (*Ln* = Tb, Dy, and Ho) phases were obtained via the thermal decomposition of *Ln*(SO4)F•H2O (*Ln* = Tb, Dy, and Ho). Unlike the *Ln*(SO4)F•H2O (*Ln* = Nd, Tb, Dy, and Ho) phases that are isostructural, two different structures are reported for the *Ln*SO4F (*Ln* = Tb, Dy, and Ho) series and, accordingly, we suggest one structure for Tb and one structure for Dy and Ho, differing in the rare earth coordination environments. Green photoluminescence is observed for $Tb(SO_4)F•H_2O$ and

$Tb(SO_4)F$. Magnetic measurements indicate the absence of magnetic order down to 2K in the $Ln(SO_4)F•H_2O$ and $Ln(SO_4)F$ phases.

Acknowledgements

Financial support for this work was provided by the National Science Foundation under DMR-2221403 and is gratefully acknowledged.

Supporting Information

The Supporting Information is available free of charge at ???

Atomic positions and Isotropic Displacement Parameters for $Ln(SO_4)F$ (*Ln* = Tb, Dy, and Ho), powder X-ray diffraction patterns, and Infrared spectra.

Accession Codes

CCDC 2407417, 2407418, 2407419, and 2407420 contain the supplementary crystallographic data for this paper. These data can be obtained free of charge via www.ccdc.cam.ac.uk/data_request/cif, or by emailing data_request@ccdc.cam.ac.uk, or by contacting The Cambridge Crystallographic Data Centre, 12 Union Road, Cambridge CB2 1EZ, UK; fax: +44 1223 336033.

References

1. Blasse, G. Scintillator Materials. *Chem. Mater.* **1994**, *6*, 1465-1475.
2. Council, N. R.; Engineering, D. O.; Sciences, P.; Physics, B. O.; of, C. F. A. A.; Synthesis, O. F. N. M.; Growth, C. *Frontiers in Crystalline Matter: From Discovery to Technology*; National Academies Press: 2009.
3. Hirai, D.; Climent-Pascual, E.; Cava, R. J. Superconductivity in $WO_{2.6}F_{0.4}$ Synthesized by Reaction of WO_3 with Teflon. *Phys. Rev. B.* **2011**, *84*, 174519.
4. Krizan, J. W.; Cava, R. J. $NaCaCo_2F_7$: A Single-Crystal High-Temperature Pyrochlore Antiferromagnet. *Phys. Rev. B.* **2014**, *89*, 214401.
5. Carone, D.; Klepov, V. V.; Misture, S. T.; Schaeperkoetter, J. C.; Jacobsohn, L. G.; Aziziha, M.; Schorne-Pinto, J.; Thomson, S. A. J.; Hines, A. T.; Besmann, T. M., zur Loye, H.-C. Luminescence and Scintillation in the Niobium Doped Oxyfluoride $Rb_4Ge_5O_9F_6$: Nb. *Inorganics.* **2022**, *10*, 83.
6. Ayer, G. B.; Klepov, V. V.; Smith, M. D.; Hu, M.; Yang, Z.; Martin, C. R.; Morrison, G.; zur Loye, H.-C. $BaWO_2F_4$: a Mixed Anion X-ray Scintillator with Excellent Photoluminescence Quantum Efficiency. *Dalton Trans.* **2020**, *49*, 10734-10739.
7. Aslani, C. K.; Klepov, V. V.; zur Loye, H.-C. Flux Crystal Growth of a New $BaTa_2O_6$Polymorph, and of the Novel Tantalum Oxyfluoride Salt Inclusion Phase $[Ba_3F]Ta_4O_{12}F$: Flux Dependent Phase Formation. *J. Solid State Chem.* **2021**, *294*, 121833.
8. Latshaw, A. M.; Wilkins, B. O.; Hughey, K. D.; Yeon, J.; Williams, D. E.; Tran, T. T.; Halasyamani, P. S.; zur Loye, H.-C. $A_5RE_4X[TO_4]_4$ Crystal Growth and Photoluminescence. Fluoride Flux Synthesis of Sodium and Potassium Rare Earth Silicate Oxyfluorides. *CrystEngComm.* **2015**, *17*, 4654-4661.
9. Morrison, G.; Klepov, V. V.; zur Loye, H.-C. Pentanary Cesium Titanyl/Titanate Silicate Oxyfluorides: Syntheses and structures. *Solid State Sci.* **2021**, *118*, 106664.
10. Latshaw, A. M.; Wilkins, B. O.; Morrison, G.; Smith, M. D.; zur Loye, H.-C. $A_5RE_4X[TO_4]_4$ Crystal Growth: Fluoride Flux Synthesis of $Na_5Ln_4F[GeO_4]_4$ (Ln= Pr, Nd), the First Quaternary Germanate Oxyfluorides. *J. Solid State Chem.* **2016**, *239*, 200-203.
11. Yeon, J.; Felder, J. B.; Smith, M. D.; Morrison, G.; zur Loye, H.-C. Synthetic Strategies for New Vanadium Oxyfluorides Containing Novel Building Blocks: Structures of V(iv) and V(v) Containing $Sr_4V_3O_5F_{13}$, $Pb_7V_4O_8F_{18}$, $Pb_2VO_2F_5$, and Pb_2VOF_6. *CrystEngComm.* **2015**, *17*, 8428-8440.
12. Grzyb, T.; Wiglusz, R. J.; Nagirnyi, V.; Kotlov, A.; Lis, S. Revised Crystal Structure and Luminescent Properties of Gadolinium Oxyfluoride $Gd_4O_3F_6$ Doped with Eu^{3+} Ions. *Dalton Trans.* **2014**, *43*, 6925-6934.
13. Passuello, T.; Piccinelli, F.; Trevisani, M.; Giarola, M.; Mariotto, G.; Marciniak, L., D; Guzik, M.; Fasoli, M.; Vedda, A.; Jary, V.; Nikl, M.; Causin, V.; Bettinelli, M., A. Structural and Optical Properties of Vernier Phase Lutetium Oxyfluorides Doped with Lanthanide Ions: Interesting Candidates as Scintillators and X-ray Phosphors. *J. Mater. Chem.* **2012**, *22*, 10639-10649.
14. Lisha, L. I. U.; Haohong, C. H. E. N.; Biqiu, L. I. U.; Hui, Z. H. A. N. G.; BiN, T. A. N. G.; Xianjuan, F. E. N. G.; Zhijia, S. U. N.; Jingtai, Z. H. A. O. Synthesis, Structure and Luminescent Properties of a New Vernier Phase $Lu_7O_6F_9$ Doped by Eu^{3+} as Potential Scintillator with Unique Lath Tube Architecture. *J. Rare Earths.* **2014**, *32*, 686-690.

15. Yahia, H. B.; Shikano, M.; Kobayashi, H.; Avdeev, M.; Liu, S.; Ling, C. D. Structural Relationships among LiNaMg[PO_4] F and $Na_2M[PO_4]F$ (M= Mn–Ni, and Mg), and the Magnetic Structure of LiNaNi[PO_4]F. *Dalton Trans.* **2014**, *43*, 2044-2051.
16. Leblanc, M.; Collin-Fèvre, I.; Férey, G. The Magnetic Structures of Mn_2PO_4F and Co_2PO_4F at 1.2 K. *J. Magn. Magn. Mater.* **1997**, *167*, 71.
17. Zhen, N.; Wu, K.; Li, Q.; Pan, S.; Gao, W.; Yang, Z. Synthesis, Structures, and Properties of Two Magnesium Silicate Fluorides $Mg_5(SiO_4)_2F_2$ and $Mg_3SiO_4F_2$. *New J. Chem.* **2015**, *39*, 8866-8873.
18. Morrison, G.; Latshaw, A. M.; Spagnuolo, N. R.; zur Loye, H.-C. Observation of Intense X-ray Scintillation in a Family of Mixed Anion Silicates, $Cs_3RESi_4O_{10}F_2$(RE = Y, Eu–Lu), Obtained via an Enhanced Flux Crystal Growth Technique. *J. Am. Chem. Soc.* **2017**, *139*, 14743-14748.
19. Schneemeyer, L. F.; Guterman, L.; Siegrist, T.; Kowach, G. R. Synthesis and Structure of a New Germanate Fluoride: $NaCa_2GeO_4F$. *J. Solid State Chem.* **2001**, *160*, 33-38.
20. Rahaman, B.; Saha-Dasgupta, T. Electronic Structure and Microscopic Model of $V_2GeO_4F_2$—a Quantum Spin System with S= 1. *J. Phys.: Condens. Matter.* **2007**, *19*, 296206.
21. Mori, D.; Yahia, H. B.; Shikano, M.; Imanishi, N.; Inaguma, Y.; Belharouak, I. Low Temperature Synthesis, Structure and Magnetic Properties of $Mn_2[VO_4]F$. *J. Asian Ceram. Soc.* **2017**, *5*, 460-465.
22. Wu, T.; Jiang, X.; Zhang, Y.; Wang, Z.; Sha, H.; Wu, C.; Lin, Z.; Huang, Z.; Long, X.; Humphrey, M. G. From $CeF_2(SO_4)\cdot H_2O$ to $Ce(IO_3)_2(SO_4)$: Defluorinated Homovalent Substitution for Strong Second-Harmonic-Generation Effect and Sufficient Birefringence. *Chem. Mater.* **2021**, *33*, 9317-9325.
23. Marshall, K. L.; Wang, Q.; Sullivan, H. S. I.; Weller, M. T. Synthesis and Structural Characterisation of Transition Metal Fluoride Sulfates. *Dalton Trans.* **2016**, *45*, 8854-8861.
24. Huang, X.; Zhang, M.; Li, J.; Zhao, Z.; He, Z. Synthesis, Crystal Structures and Physical Properties of Two New Sulfates $KYb(SO_4)_2\cdot H_2O$ and $KYb(SO_4)F_2$. *J. Solid State Chem.* **2021**, *294*, 121822.
25. Wickleder, M. S. $LiLa_2F_3(SO_4)_2$ und $LiEr_2F_3(SO_4)_2$: Fluoridsulfate der Selten-Erd-Elemente mit Lithium. *Z. Anorg. Allg. Chem.* **1999**, *625*, 302-308.
26. Wickleder, M. S. Halogenidsulfate des Gadoliniums: Synthese und Kristallstruktur von $GdClSO_4$ und $GdFSO_4$. *Z. Anorg. Allg. Chem.* **1999**, *625*, 725-728.
27. Dong, X.; Long, Y.; Zhao, X.; Huang, L.; Zeng, H.; Lin, Z.; Wang, X.; Zou, G. $A_6Sb_4F_{12}(SO_4)_3$ (A= Rb, Cs): Two Novel Antimony Fluoride Sulfates with Unique Crown-like Clusters. *Inorg. Chem.* **2020**, *59*, 8345-8352.
28. Jiao, D.-X.; Zhang, H.-L.; Li, X.-F.; He, C.; Li, J.-H.; Wei, Q.; Yang, G.-Y. $YSO_4F\cdot H_2O$: A Deep-Ultraviolet Birefringent Rare-Earth Sulfate Fluoride with Enhanced Birefringence Induced by Fluorinated Y-Centered Polyhedra. *Inorg. Chem.* **2023**, *62*, 17333-17340.
29. Lu, J.; Li, Y.; Kuk, Y.; Choi, S.; Kim, K.; Ko, C.; Bai, Z.; Ok, K. M. $Bi(SO_4)F\cdot H_2O$ and $Bi(SO_4)(NO_3)\cdot 3H_2O$: Chemical Substitution-Induced Birefringence Enhancement in Bismuth Sulfates. *Inorg. Chem.* **2024**, *63*, 13748-13754.
30. Wu, C.; Wu, T.; Jiang, X.; Wang, Z.; Sha, H.; Lin, L.; Lin, Z.; Huang, Z.; Long, X.; Humphrey, M. G. Large Second-Harmonic Response and Giant Birefringence of $CeF_2(SO_4)$ Induced by Highly Polarizable Polyhedra. *J. Am. Chem. Soc.* **2021**, *143*, 4138-4142.

31. Keerthisinghe, N.; Morrison, G.; zur Loye, H.-C. Crystal Growth and Characterization of the Rare Earth Fluoride Carbonates $NaLnCO_3F_2$ (Ln = Eu–Lu). *Cryst. Growth Des.* **2024**, *24*, 6845-6850.
32. APEX3 Version 2019.1-0 and SAINT+ Version 8.40A. **2019**,
33. Krause, L.; Herbst-Irmer, R.; Sheldrick, G. M.; Stalke, D. Comparison of Silver and Molybdenum Microfocus X-ray Sources for Single-Crystal Structure Determination. *J. Appl. Crystallogr.* **2015**, *48*, 3-10.
34. Sheldrick, G. M. SHELXT– Integrated Space-Group and Crystal-Structure Determination. *Acta Cryst. A.* **2015**, *71*, 3-8.
35. Dinnebier, R. E.; Leineweber, A.; Evans, J. S. O. *Rietveld refinement: practical powder diffraction pattern analysis using TOPAS*; Walter de Gruyter GmbH & Co KG: Berlin, Boston, 2018.
36. Morrison, G.; zur Loye, H.-C. Simple Correction for the Sample Shape and Radial Offset effects on SQUID Magnetometers: Magnetic Measurements on Ln_2O_3 (Ln=Gd, Dy, Er) Standards. *J. Solid State Chem.* **2015**, *221*, 334-337.
37. Morrison, G.; Masachchi, L. W.; Tisdale, H. B.; Chang, T.; Jones, V. G.; Zamorano, K. P.; Breton, L. S.; Smith, M. D.; Chen, Y.-S.; zur Loye, H.-C. Polymorphism in A_3MF_6(A = Rb, Cs; M = Al, Ga) Grown using Mixed Halide Fluxes. *Dalton Trans.* **2023**, *52*, 8425-8433.
38. Wang, X.; Liu, L.; Ross, K.; Jacobson, A. J. Synthesis and Crystal Structures of Yttrium sulfates $Y(OH)(SO_4)$, $Y(SO_4)F$, $YNi(OH)_3(SO_4)$-II and $Y_2Cu(OH)_3(SO_4)_2F{\bullet}H_2O$. *Solid State Sci.* **2000**, *2*, 109-118.
39. Shannon, R. D. T.; Prewitt, C. T. Effective Ionic Radii in Oxides and Fluorides. *Acta Crystallogr., Sect. B: Struct. Crystallogr. Cryst. Chem.* **1969**, *25*, 925-946.
40. Klepov, V. V.; Pace, K. A.; Breton, L. S.; Kocevski, V.; Besmann, T. M.; zur Loye, H.-C. Nearly Identical but not Isotypic: Influence of Lanthanide Contraction on $Cs_2NaLn(PS_4)_2$ (Ln= La–Nd, Sm, and Gd–Ho). *Inorg. Chem.* **2020**, *59*, 1905-1916.
41. Yang, H.; Xu, C.; Li, Z.; Li, M.; Liu, G. Synthesis, Characterization and Optical Properties of Three Novel Lanthanide Sulfates. *J. Solid State Chem.* **2021**, *303*, 122481.
42. Hines, A. T.; Morrison, G.; Yarbrough, B. J.; Shustova, N. B.; Jacobsohn, L. G.; zur Loye, H.-C. Luminescence of Alkali Rare Earth Borates $A_3Ln(BO_3)_2$ (A= Na, K; Ln= Eu, Tb). *Solid State Sci.* **2023**, *138*, 107130.
43. Jiang, N.; La Pierre, H. S. Frustrated Magnetism in a 2-D Ytterbium Fluoride. *Inorg. Chem.* **2019**, *58*, 12152-12156.

For Table of Content Use Only

Synthesis of Mixed Anion Rare Earth Sulfate Fluorides $Ln SO_4F \cdot H_2O$ (Ln = Nd, Tb, Dy, Ho) and $Ln SO_4F$ (Ln = Tb, Dy, Ho)

Lakshani W. Masachchi, Gregory Morrison, and Hans-Conrad zur Loye*

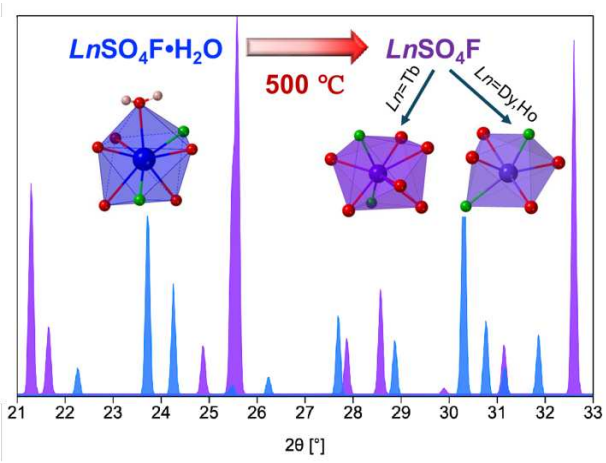

Synopsis
A series of $Ln(SO_4)F \cdot H_2O$ was prepared via an HF-free mild hydrothermal synthesis and the $Ln SO_4F$ phases were obtained via the thermal decomposition of $Ln(SO_4)F \cdot H_2O$. Their crystal structures and magnetic, thermal, and optical properties are discussed.